A Single-Period Voltage-Mode-Boosted Current-Mode Wireless Power Transfer System for Cryo-Quantum Interfaces with 5.3× VCR Improvement and 91% PCE

Yating Zou*, Tianqi Lu§, Jie Wang‡, Zenghui Li‡,
Eduard Alarcón†, Sijun Du§, Fabio Sebastiano‡, Masoud Babaie‡, Edoardo Charbon*
*Department of Microsystems and Microelectronics, École Polytechnique Fédérale de Lausanne, Switzerland
§Department of Microelectronics, Delft University of Technology, The Netherlands
‡Department of Quantum and Computing Engineering & QuTech, Delft University of Technology, The Netherlands
†School of Telecommunications, Technical University of Catalunya, Spain
yating.zou@epfl.ch

***Abstract*—This paper presents a wireless power transfer system comprising a transmitter and a voltage-mode-boosted current-mode (VB-CM) receiver. To achieve both high voltage conversion ratio (VCR) and power conversion efficiency (PCE) in weak coupling situations, the proposed VB-CM receiver enables single-period resonance by reusing an internal voltage from the voltage-mode operation to boost the current-mode resonance. To maintain high PCE over an extended operating temperature range from 300 K to 4 K, a closed-loop successive-approximation- register (SAR)-based boosting-time control is proposed to compensate for temperature-dependent transistor behavior. The system is fabricated in a 40-nm CMOS technology and supports dual outputs of 1 V/15 mW and 2.5 V/87.5 mW. With single-period resonance, the receiver achieves 5.3× VCR enhancement at both 300 K and 4 K, along with peak PCE of 91% at 4 K and 87% at 300 K.**

***Keywords*—Wireless power transfer (WPT), voltage-mode-boosted current-mode (VB-CM), single-period resonance, cryogenic temperature.**

I. Introduction

Wireless power transfer (WPT) is a promising approach for powering biomedical implants at room temperature (RT), enabling long-term safety [1], and for quantum systems at cryogenic temperature (CT), where it mitigates heating associated with wired conduction [2] as shown in Fig. 1(a). Nonetheless, the WPT system faces three key challenges: 1) weak coupling caused by coil misalignment or long transfer distance; 2) thermal stress that destabilizes the temperature environment; 3) the need for multiple independent power supplies to support various functional blocks. As shown in Fig. 1(b), high voltage conversion ratio (VCR) for low input at the RX is required to compensate for weak coupling. Meanwhile, high power conversion efficiency (PCE) is essential to minimize thermal stress in implantable systems or cryogenic quantum platforms. Furthermore, temperature-dependent transistor behavior can degrade PCE. To keep high

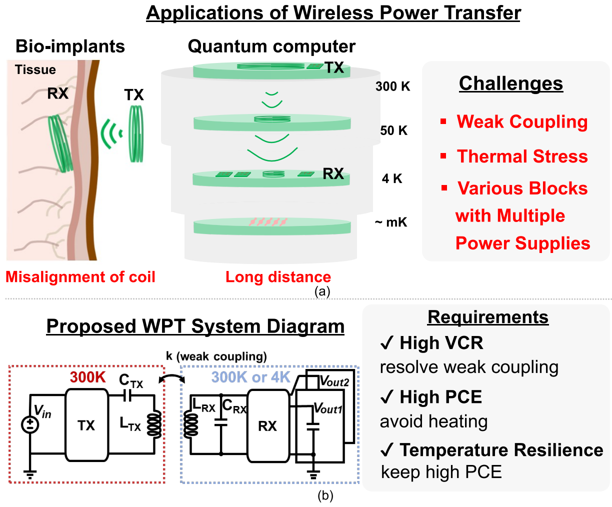

Fig. 1. (a) Wireless power transfer (WPT) applications, and (b) proposed WPT system.

PCE across a wide temperature range, a temperature-resilient receiver (RX) is therefore required.

As shown in Fig. 2, conventional approaches to improve VCR are based on a current-mode (CM) RX [3], which receives low power with weak coupling, resonates for multiple periods, and subsequently transfers high power to the load, achieving high VCR. However, this method suffers from the on-resistance loss of the switch in LC resonance tank for multiple periods, and thus achieves poor PCE. Another method is based on a voltage-mode (VM) RX [4], which has favorable PCE by removing the power switch in the LC tank. Nevertheless, VM rectification induces a limited VCR (< 1), making it unsuitable for weak coupling applications in a dilution fridge. On the other hand, multiple power supplies for quantum-classical interfaces are required for various blocks

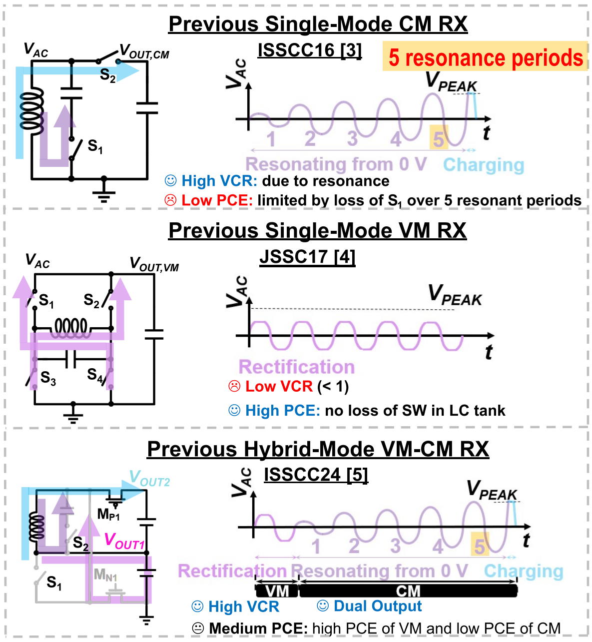

Fig. 2. Previous single-mode RXs and hybrid-mode RXs.

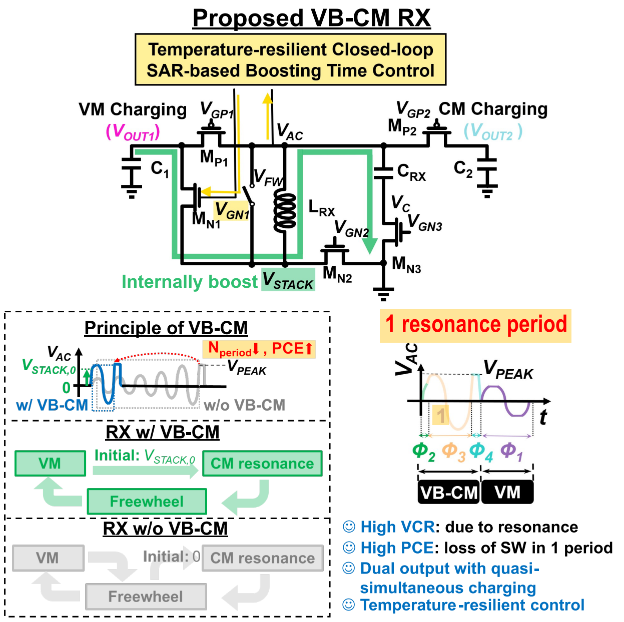

Fig. 3. Proposed VB-CM RX topology and operational principle.

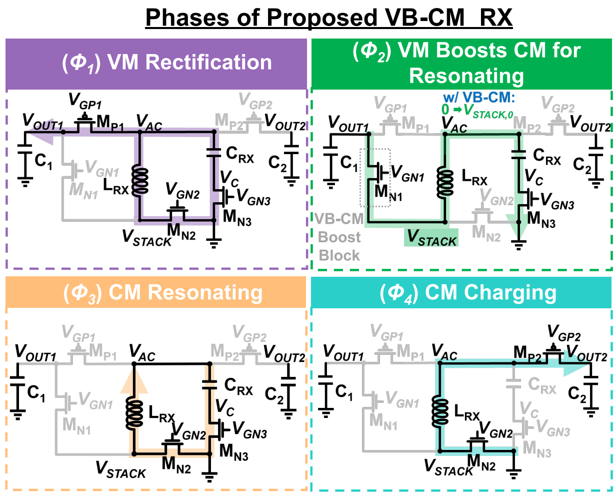

Fig. 4. Operation phases of proposed VB-CM RX.

such as digital and analog units. However, existing hybrid-mode dual-output RXs (e.g., VM–CM [5], VM–VM [6], CM–CM [7]) only enable two modes to operate separately, making it difficult to achieve high VCR and PCE simultaneously.

This paper proposes a WPT system comprising a transmitter (TX) and a dual-output voltage-mode–boosted current-mode (VB–CM) RX, enabling the VM stage to boost the CM stage with negligible impact on the VM output voltage. The RX breaks the trade-off between VCR and PCE by operating within a single resonance period while accommodating temperature variations. Section II shows the principle of the proposed RX. Section III presents the circuit implementation. Measurement results are discussed in Section IV, followed by the conclusion in Section V.

II. Proposed Voltage-Mode-Boosted Current-Mode (VB-CM) RX

Fig. 3 shows the proposed VB-CM RX. The principle of VB-CM RX is reusing an internally generated stacked voltage $V_{\mathrm{STACK},0}$ from VM output to pre-charge the CM tank by enabling M_{N1} before CM resonance. Unlike conventional CM RXs (without VB–CM) that resonate from zero, this proposed VB-CM RX initiates resonance from a nonzero initial voltage, suffers on-resistance loss in single-cycle operation instead of multiple resonance periods and thereby improving PCE.

On the other hand, unlike previous VM RX, the proposed VB-CM RX relies on resonance rather than rectification, enabling a higher achievable VCR under weak coupling. Owing to the single-period resonance, the proposed RX enables dual-output operation with quasi-simultaneous charging. To optimize PCE over a wide temperature range, a closed-loop successive-approximation-register (SAR)-based boosting-time control is proposed, as shown in Fig. 3. The duty cycle of V_{GN1} defines the pre-charge interval from the VM stage to the CM stage. It is determined by the comparator and delay cell and is sensitive to threshold voltage and carrier mobility, making it temperature dependent. The closed-loop control ensures an optimal pre-charge duration, thereby maintaining high PCE across temperatures.

III. System and Circuit Implementations

Fig. 4 shows the four phases of the VB-CM RX, and Fig. 5 shows the RX waveforms without and with VB-CM. The proposed RX integrates VM and CM stages sharing an LC tank to generate V_{OUT1} and V_{OUT2}. VM operates in Φ_1, while CM operates in Φ_3 and Φ_4. Φ_2 serves as an intermediate phase to

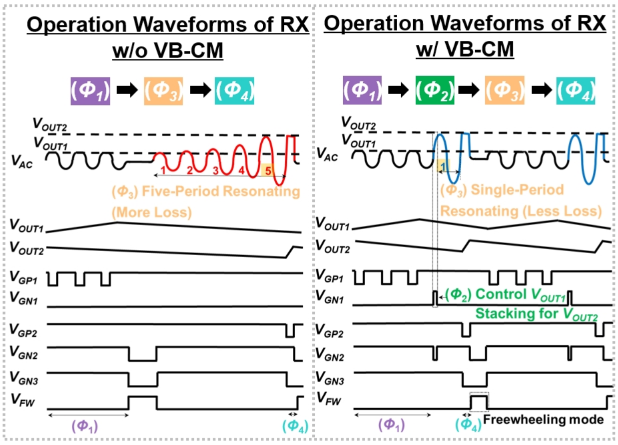

Fig. 5. Operation waveforms of RX w/o VB-CM and RX w/ VB-CM.

reuse the VM output to boost the CM resonance. Accordingly, the RX without VB–CM includes Φ_1, Φ_3, and Φ_4, while the proposed VB–CM RX includes all four phases.

During the VM rectification phase (Φ_1) shown in Fig. 4(b), M_{P1}, M_{N2}, and M_{N3} are turned on, forming a VM rectifier together with the receiver coil L_{RX} and capacitor C_{RX}. Given the low VCR and high PCE of this VM rectifier, V_{OUT1} supplies a low-power rail (1 V). During the boosted phase (Φ_2), M_{N1} and M_{N3} are turned on, and V_{OUT1} is stacked onto L_{RX} for ∼20 ns to provide an initial voltage $V_{STACK,0}$. After removing V_{OUT1}, L_{RX} still maintains current continuity and generate voltage for V_{OUT2}. During the resonant phase (Φ_3), M_{N2} and M_{N3} are turned on, and the LC tank resonates in the CM stage. Owing to the stacked voltage from the VM stage, V_{AC} resonates from $V_{STACK,0}$ rather than zero, enabling the VM stage to boost the CM stage and allowing V_{OUT2} to reach the threshold V_{PEAK} within a single period. Therefore, efficiency losses through M_{N2} and M_{N3} only occur in the single period, ensuring both high VCR and PCE. The RX enters the CM charging phase (Φ_4) and M_{P2} is turned on, once V_{AC} surpasses the threshold V_{PEAK}. All the energy stored in L_{RX} is then transferred to C_2 with a high supply voltage (2.5 V).

Fig. 6 shows the circuit implementation of the RX control circuits and class-D TX. During phase Φ_2, M_{N1} is driven by V_{GN1}, thereby connecting M_{N1} onto L_{RX}. However, from 300 K to 4 K, the threshold voltage of the transistor shifts by hundreds of millivolts and the carrier mobility increases by 2-5×, making the duty cycle of V_{GN1} unpredictable. An optimum duty cycle is required to avoid a significant V_{OUT1} drop and ensure sufficient stacking onto the CM stage. Therefore, to compensate for the temperature-dependent duty-cycle variation, a closed-loop SAR-based boosting-time control is proposed. The control signal V_{CTR_DELAY} is generated by a comparator comparing V_{AC} and V_{AC_H} to extract the rising interval of V_{AC}. $V_{CTR\_PEAK\_D}$ is a delayed version of V_{CTR_PEAK}. Their AND output sets the minimum duty cycle of V_{GN1}, which is regulated by a counter and SAR logic to tune the delay cell. During Φ_4, L_{RX} delivers current to V_{OUT2}. Charging begins at the peak of I_{AC}, and M_{P2} transitions from short-circuit to diode mode. The charging phase terminates automatically when I_{AC} falls to zero.

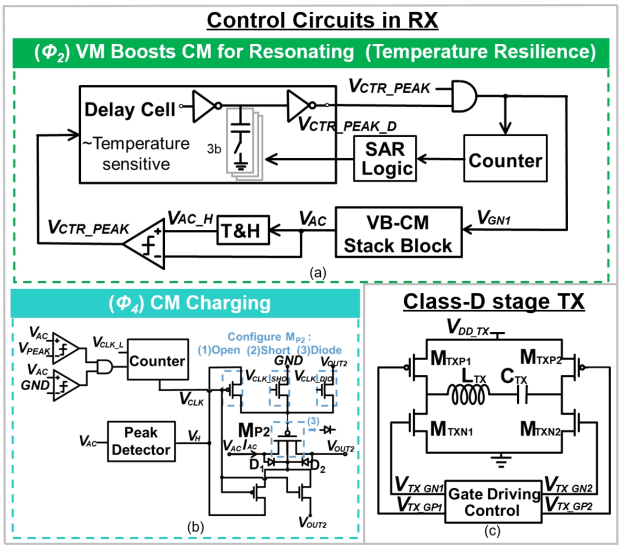

Fig. 6. Circuits of RX and TX: (a) control circuits for Φ_2 in RX, (b) control circuits for Φ_4 in RX, and (c) circuits of proposed TX.

IV. Measurement Results

The proposed TX and RX were fabricated in a 40-nm CMOS process, as shown in Fig. 7(a) and (b). The RX was mounted in the 4-K or 300-K stage of a probe station and interfaced with the TX at 300 K in Fig. 8(a) and (b).

Fig. 9(a) and (b) show the measured steady-state waveforms of the RX interfaced with the TX under load conditions with $I_{OUT1} = 15$ mA and $I_{OUT2} = 35$ mA, corresponding to maximum peak load powers of 15 mW and 87.5 mW, respectively. The VM rectification and CM resonance stages in RX generate the output voltages V_{OUT1} and V_{OUT2} at 1 V and 2.5 V, respectively. Compared with 300 K, the on-resistance loss increases at 4 K due to elevated threshold voltage and enhanced carrier mobility, while the receiver-coil quality factor improves from 80 to 180, reducing parasitic loss. Fig. 9(a) shows the V_{AC} waveform of the RX without VB-CM, where five resonance periods are required before charging begins, resulting in a PCE of 84%. Fig. 9(b) shows the V_{AC} waveform with VB-CM. After the VM rectification phase (Φ_1), charging begins within a single resonance period, achieving a PCE of 91% and a 7% improvement at CT. At 300 K, a 9% PCE improvement is also achieved, as shown in Fig. 9(c).

Fig. 9(d) shows the end-to-end (E2E) efficiency from the TX input to the RX output. At CT, with a 2-cm TX–RX separation across the shield window gap, where the window glass introduces significant attenuation, the maximum E2E efficiency reaches 63% at $I_{OUT1} = 15$ mA and $I_{OUT2} = 30$ mA.

As shown in Fig. 8(c) and Table I, the RX with VB-CM enables single-period resonance, allowing the RX to achieve a VCR of 5 while maintaining a PCE of 91%, corresponding to a 5.3× improvement in VCR compared to the RX with VM at 4 K. In contrast, the RX without VB-CM also attains a VCR

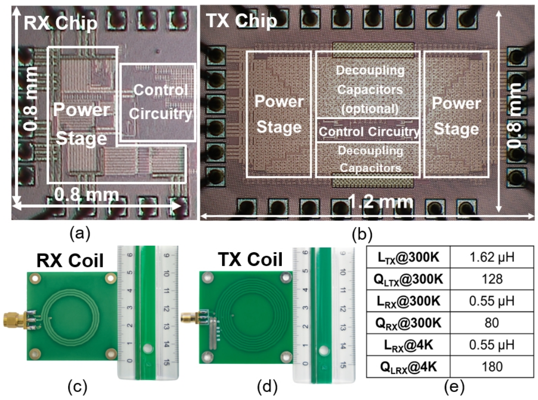

Fig. 7. (a) Die micrograph of RX, (b) die micrograph of TX, (c) RX coil, (d) TX coil, and (e) specifications of RX and TX coils.

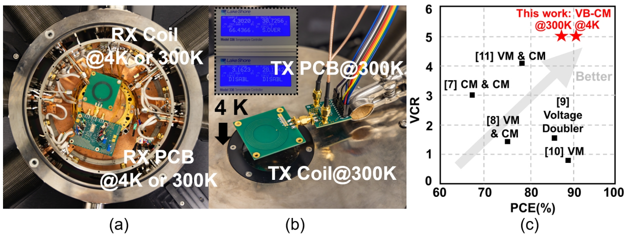

Fig. 8. (a)-(b) Measurement setup, and (c) comparison of VCR and PCE.

of 5, but with only a reduced PCE of 84% at 4 K. Compared with the state of the art, this work achieves the highest VCR of 5 while sustaining a high PCE of 91% at 4 K, and maintains the highest VCR of 5 with PCE of 87% at 300 K.

V. Conclusion

This paper presents a wireless power transfer system operating from 300 K to 4 K, comprising a transmitter and a dual-output VB–CM receiver, that breaks the trade-off between voltage conversion ratio (VCR) and power conversion efficiency (PCE). Thanks to the reuse of the internally-generated output from VM to boost CM resonance, the proposed receiver achieves single-period resonance and the highest VCR of 5 while maintaining a high PCE of 91% at 4 K, corresponding to a 5.3× VCR improvement compared to a VM-only receiver at both 300 K and 4 K. With temperature-resilient control, the system sustains high PCE and VCR across a wide temperature range, making it a suitable solution for weak-coupling implantable applications and quantum-classical interfaces.

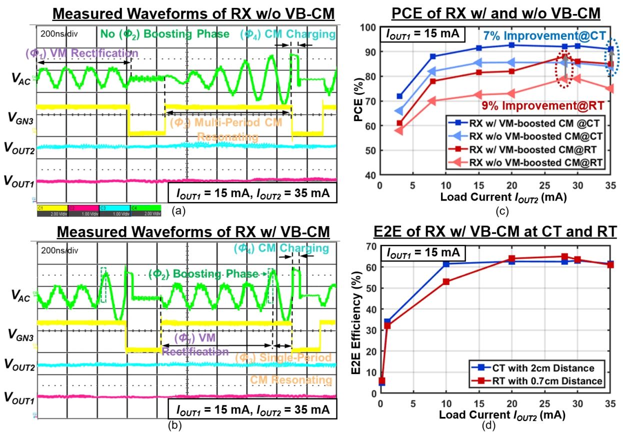

Fig. 9. Measured results: (a)-(b) measured waveforms of proposed RX w/o and w/ VB-CM, (c) PCE of RX, and (d) E2E of WPT system.

TABLE I
Performance Summary and Comparison.

Specification	This work		JSSC'20 [7]	JSSC'17 [11]	ISSCC'24 [5]	ISSCC'25 [6]
Operating Temperature	4 K	300 K	300 K	300 K	300 K	300 K
Technology	40nm CMOS		180nm CMOS	350nm CMOS	180nm CMOS	180nm CMOS
Architecture	TX & RX		RX	TX & RX	TX & RX	RX
RX Topology	VM & VM-boosted CM		CM & CM	VM & CM	VM & CM	VM & VM
Frequency (MHz)	6.78		13.56	1	13.56	6.78
Coil Diameter (cm)	TX 4; RX 3.3		RX 0.7	TX 17; RX 3	TX 3; RX 2	NO
V_{OUT}@RX (V)	2.5 ; 1		0.5-3	3.2	1.8 ; 1.8	1.6 ; 3.3
Peak P_{OUT}(mW)	102.5		47	20	80.5	109.9
VCR(@PCE & I_{OUT})	5 (@91% & 30mA)	5 (@87% & 28mA)	3 (@67.8% & NA)	4.1 (@77% & 32μA)	<2 (@90.1% & 30mA)	< 1 (@92.2% & 28mA)
E2E Efficiency(%) (@D_{coil})	63% (@2cm shield window gap)	65% (@0.7cm air gap)	NO	NA	72.3% (@0.5cm)	NO
Max. Transfer Distance D_{coil} (@I_{OUT})	3 cm window gap (@0.2mA)	7.5 cm air gap (@0.3mA)	NO	6 cm (@32μA)	7 cm (@0.18mA)	NO

Acknowledgment

All authors acknowledge support from the EU, grant HORIZON-EIC-2022-PATHFINDEROPEN-01-101099697, QUADRATURE.

References

[1] M. Kiani, "Wireless power transfer and management for medical applications: Wireless power," *IEEE Solid-State Circuits Magazine*, vol. 14, no. 3, pp. 41–52, 2022.

[2] Y. Zou *et al.*, "Power delivery for cryogenic scalable quantum applications: Challenges and opportunities," 2025, arXiv:2511.13965.

[3] M. Choi *et al.*, "21.5 a current-mode wireless power receiver with optimal resonant cycle tracking for implantable systems," in *ISSCC*, 2016, pp. 372–373.

[4] C. Huang *et al.*, "A 13.56-MHz wireless power transfer system with enhanced load-transient response and efficiency by fully integrated wireless constant-idle-time control for biomedical implants," *JSSC*, vol. 53, no. 2, pp. 538–551, Feb. 2018.

[5] T. Lu and S. Du, "27.4 a 13.56MHz wireless power transfer system with hybrid voltage-/current-mode receiver and global digital-PWM regulation achieving 150% transfer range extension and 72.3% end-to-end efficiency," in *ISSCC*, 2024, pp. 450–452.

[6] Q. Zhuang *et al.*, "9.6 a 6.78MHz single-stage regulating rectifier with dual outputs simultaneously charged in a half cycle achieving 92.2% efficiency and 131mw output power," in *ISSCC*, 2025, pp. 188–190.

[7] S.-U. Shin *et al.*, "A time-interleaved resonant voltage mode wireless power receiver with delay-based tracking loops for implantable medical devices," *JSSC*, vol. 55, no. 5, pp. 1374–1385, May 2020.

[8] H. Sadeghi Gougheri and M. Kiani, "An inductive voltage-/current-mode integrated power management with seamless mode transition and energy recycling," *JSSC*, vol. 54, no. 3, pp. 874–884, Mar. 2019.

[9] T. Lu and S. Du, "A single-stage regulating voltage-doubling rectifier for wireless power transfer," *SSCL*, vol. 6, pp. 29–32, 2023.

[10] L. Cheng *et al.*, "Adaptive on/off delay-compensated active rectifiers for wireless power transfer systems," *JSSC*, vol. 51, no. 3, pp. 712–723, Mar. 2016.

[11] H. Sadeghi Gougheri and M. Kiani, "Self-regulated reconfigurable voltage/current-mode inductive power management," *JSSC*, vol. 52, no. 11, pp. 3056–3070, Nov. 2017.